Reversible Logic with a Nanofluidic Memristor

Sergio Portillo,[a] Javier Cervera[a,*], Salvador Mafe,[a,b] Patricio Ramirez[c]

[a]Dept. de Física de la Terra i Termodinàmica, Universitat de València, E-46100 Burjassot, Spain
[b]Allen Discovery Center at Tufts University, Medford, Massachusetts 02155, USA
[c]Dept. de Física Aplicada, Universitat Politécnica de València, E-46022 València, Spain

ABSTRACT

A multipore membrane with current-rectifying nanofluidic diodes exhibits memristive properties based on the surface charge-regulated ionic transport. The neuromorphic-like potentiation of the conductance by voltage pulses provides different functionalities that can be modulated not only by the amplitude and frequency of the driving oscillatory signal but also by the ionic concentration and *pH* values of the external solutions. This fact allows to implement a broad range of logical functions by the external reconfiguration of the nanofluidic diodes. As a proof of concept, we show Boolean (*AND*, *NAND*, and *XOR*) and reversible (*Feynman*) logical functions obtained by controlling chemical (*pH* and ionic concentration) and electrical (voltage and current) signals in an electrochemical cell. The system displays some reminiscences to channel biophysics signaling in cell membranes and provides a suitable logical environment for sensing and information processing in iontronics hybrid devices. Model simulations that explain the experimental data and explore future applications are also included.

Keywords: multipore membrane, nanofluidic diode, ionic memristor, concentration and *pH*-regulated logic functions, reversible logic

* Correspondence to: Dept. de Física de la Terra i Termodinàmica, Universitat de València, E-46100 Burjassot, Spain. E-mail address: javier.cervera@uv.es (Javier Cervera)

1. Introduction

Surface charge-regulated ionic selectivity and transport in micro and nanostructures constitutes an active field of research that involves both basic [1-11] and applied [7,12-17] physical concepts. Nanofluidic diodes in multipore membranes act as memory resistors that have attracted broad attention as neuromorphic devices for signal processing and computing applications. They show concentration and *pH*-dependent properties that are central to ionic-electronic signal conversion, information processing, molecular sensing and controlled release, and energy storage [4,5,7,12-21]. In particular, memory and current-rectifying characteristics, which are determined by the interaction between the pore surface charges and the solution mobile ions, are receiving much attention [5,8,9,14,22,23]. Remarkably, many physico-chemical phenomena in memristive devices are reminiscent of those observed in ion channels, the nanoscale aqueous pores that control the transference of matter and information across the cell membrane [24,25]. Here, voltage-gated pores, concentration gradients, and membrane potentials regulate the ionic transport phenomena.

Nanofluidic diodes can also mimic synaptic functions [5,9,14,22,23]. We have described experimentally [9] and theoretically [26] the basic chemical physics of multipore memristors with conical diodes, demonstrating that series and parallel arrangements can provide robust functionalities [27]. Here, we provide a significant extension of this work by showing that a universal Boolean function (*NAND*) and a reversible logic function (*Feynman*) can be implemented on the basis of the rectifying and memristive properties. As in the biological case, the neuromorphic-like potentiation of the membrane conductance is modulated not only by the voltage pulse characteristics (amplitude and frequency of the *input* signal) but also by the asymmetries of both the membrane and the external solutions. This experimental fact confirms that memristive membranes can be arranged in electrochemical circuits for information processing in iontronics, an emerging field that use ionic solutions in signal

processing phenomena, usually relating artificial platforms to biological systems. In this context, the existing links between biological ion channels and liquid-state ionic memristors should facilitate signal conversion in bioengineering and health sciences, where the combination of electrical and chemical signals modulate multitude of logical responses [7,10,12-16,18]. For the sake of completeness, suggestions for future experimental work and theoretical simulations are also included to guide the exploration of new applications.

2. Experimental

The multipore membrane characteristics have been described in detail previously [9]. Irradiation of a 12.5 μm thick polyimide foil by swift heavy ions and track functionalization by asymmetric track-etching techniques [28,29] gives conical nanopores of tip and base radii of the order of 10 nm and 100 nm, respectively [30]. Because of the functionalized chains on the pore surface, the pore is negatively charged at $pH = 7.0$ and positively charged at $pH = 1.5$ [30]. The electrical conductance potentiation is measured with the membrane mounted in a home-made electrochemical cell equipped with a pair of Ag|AgCl electrodes that are connected to a BioLogic SP-200 potentiostat. The electrode in the solution facing the pore base is the reference electrode.

To avoid electrical and mechanical perturbations, the cell is located within a magnetic shield and placed on an anti-vibration table. The multipore membrane has about 300 pores over an exposed area of 1 cm^2 approximately and is immersed between two external solutions of pH values pH_{tip} and pH_{base} and ionic concentrations c_{tip} and c_{base}. Here, a broad range of pH values and salt concentrations are considered both in symmetrical and asymmetrical external solutions. in some cases, ion concentrations or pHs at pore tip, base and external solutions are held at different values. During the experiments, the ionic concentration and pH values in the two

external solutions are approximately constant because of the small fluxes obtained through the nanopores and the relatively large reservoir volumes of the electrochemical cell.

3. Results and discussion

The current (I) – voltage (V) curves of Fig. 1(a) show clear rectifying and memristive ionic conduction characteristics [9,26]. The rectifying properties are due to the fixed charges located on the conical pore surface, which give an asymmetric volume charge distribution and a strongly nonlinear axial profile of the electric potential across the pore, especially at the nanoscale pore tip [31]. Here, the membrane fixed charges are carboxylic acid groups which are deprotonated at $pH = 7$, giving surface densities in the range between −0.1 and −1.0 e/nm^2, where e is the elementary charge [31]. Because of the negative pore charges, the mobile cations accumulate at the cone tip for $V > 0$, giving a high pore conductance (Fig. 1(b)). On the contrary, the cations are depleted at the tip for $V < 0$, giving a low pore conductance [31]. The pore charge can become positive at $pH = 1.5$, thus reversing the current rectification in Fig. 1(b), as shown previously [30]. Fig. 1(c) suggests that other $I-V$ curves and membrane electrical functionalities can be implemented by imposing a pH difference in the external solutions.

The memristive properties arise when the ionic solution at the cone tip cannot follow instantaneously the changes of the driving voltage signal with time [26,32]. When the pore charge gradient in the membrane follows the ionic concentration gradient imposed in the external solutions, the concentrated solution faces the pore tip and thus the conductance memory effects are large (Fig. 1(a)) [33]. On the contrary, when the diluted solution faces the pore tip, the number of ions involved in the voltage switching is reduced, and thus the memristive effects are small (Fig. 1(a)). Figs. 1(b) and 1(c) shows also the different memory responses obtained by changing the pH of the external solutions, which modulate the sign of the pore charges and the ion accumulation/depletion phenomena at the pore tip [26,32-36]. This

experimental fact provides an additional switching control of the membrane properties in sensing and information processing applications. The figure insets schematically show the pore surface charge and the majority mobile ion. In each case, the flux direction depends on the particular ion charge and follow the sign of the applied voltage, as explained previously [30,31].

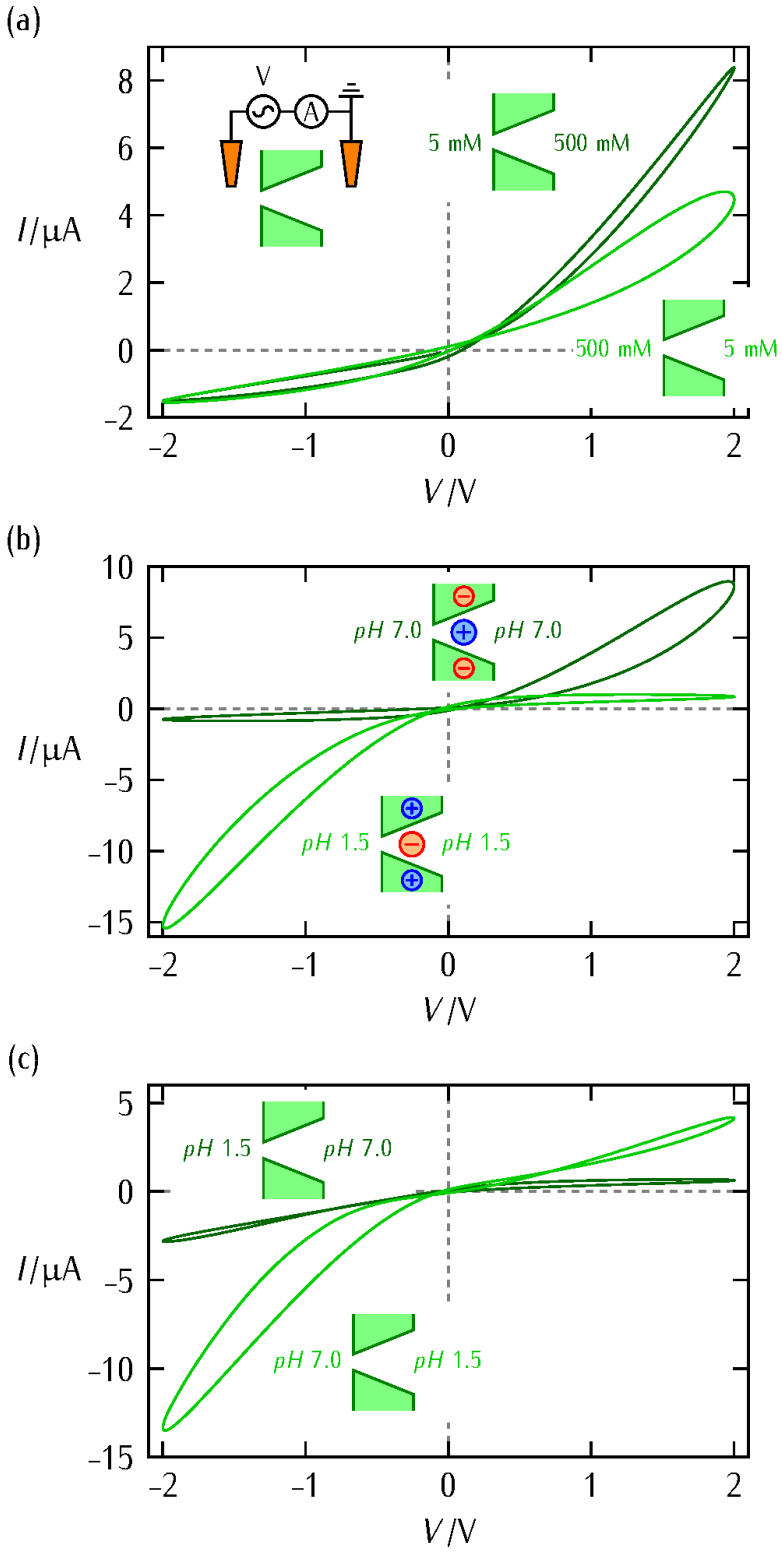

Fig. 1. (a) $I - V$ curves for two configurations of the pore tip-base concentration difference, $c_{tip} < c_{base}$ and $c_{tip} > c_{base}$. (b) $I - V$ curves for two pH values, $pH_{tip} = pH_{base}$, in symmetrical external solutions. (c) $I - V$ curves for two configurations of the pore tip-base pH difference in

asymmetrical external solutions. In all cases, the external solutions have a 100 mM KCl concentration. Note the voltage sign and the electrodes position together with the pore surface charge and majority mobile ion schemes.

The combination of the rectifying and memristive characteristics of Figs. 1(a)–1(c) allows the implementation of a logical function system on the basis of the conductance potentiation/depression phenomena induced by sequences of voltage pulses. When the membrane conductance (*output*) is modulated by the signs of the electric potential and concentration differences (*inputs*), an *AND* Boolean response is obtained (Fig. 2). The memristive nanofluidics of Fig. 1(a) allows then logical *inputs* and *outputs* based on the combination of chemical signals with sequences of positive or negative electrical potential pulses, an alternative to the timing and responses characteristic of purely electrical steady-state logics. While the voltage V and the concentration difference $c_{tip}-c_{base}$ give an *AND* logic response in terms of the membrane conductance G (Fig. 2), other logical responses potentially useful for iontronic circuits [10,12,14,15,16,18,34] can also be obtained.

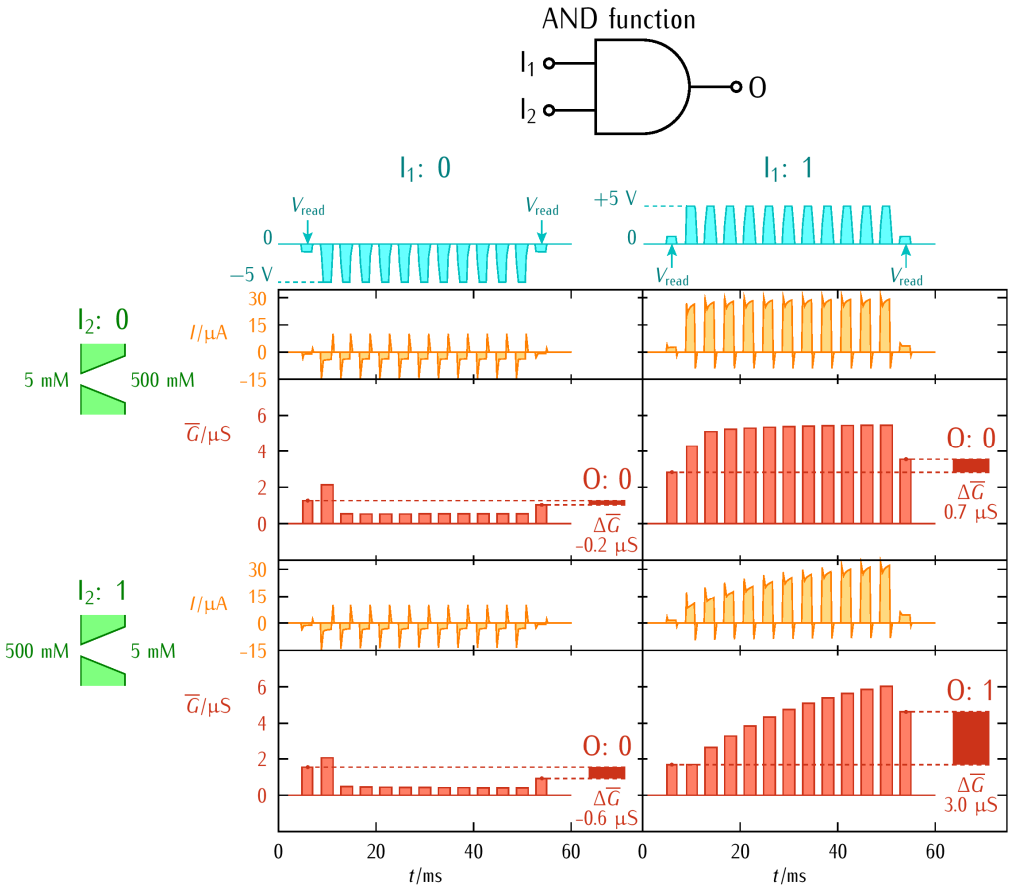

Fig. 2. The voltage V and the concentration difference c_{tip}–c_{base} (*inputs* I_1 and I_2) give an *AND* logic response in terms of the membrane conductance (*output* O) for the case of $pH_{tip} = pH_{base} = 7$. The correspondence of *inputs* 0 and 1 with the concentration difference (*left*) and voltage (*top*) values is shown. The sequences of negative (*input* 0) and positive (*input* 1) voltage pulses of amplitude $V_0 = 5$ V, duration of 2 ms, and intervals of 2 ms give the current I *vs.* time t curves shown. The average conductance $\overline{G}$ characteristic of every pulse is calculated from the ratio between the current and the pulse potential. The small voltage amplitudes (V_{read}) applied at the beginning and at the end of each pulse sequence permit to evaluate the average conductance difference $\Delta\overline{G}$ that characterizes the membrane response for the different configurations. In this case, only one conductance potentiation is obtained. To obtain a conductance difference that allows the implementation of the logical *output* 1, the number of pulses must be high

enough for the potentiation effect to be noticeable. Here, we have checked that 11 pulses are generally enough to achieve reliable logical responses.

Figs. 1(b) and 1(c) show that the *pH* values of the external solutions, which modulate the sign of the pore charges and the ion accumulation/depletion phenomena at the pore tip [26,35,36], can also be used as a logical *input*. For instance, the combined action of the voltage V and *pH* in the tip solution gives a universal *NAND* logical response in terms of the different initial and final conductances obtained at the beginning and the end of the pulse sequences (Fig. 3). In this case, we take the sign of the voltage V as the first *input* variable, fix $pH_{base} = 1.5$, and take pH_{tip} as the second *input* ($pH_{tip} = 7.0$ for *input* 0 and $pH_{tip} = 1.5$ for *input* 1). The output variable is *output* 0 for no conductance potentiation and *output* 1 for conductance potentiation, as in Fig. 2.

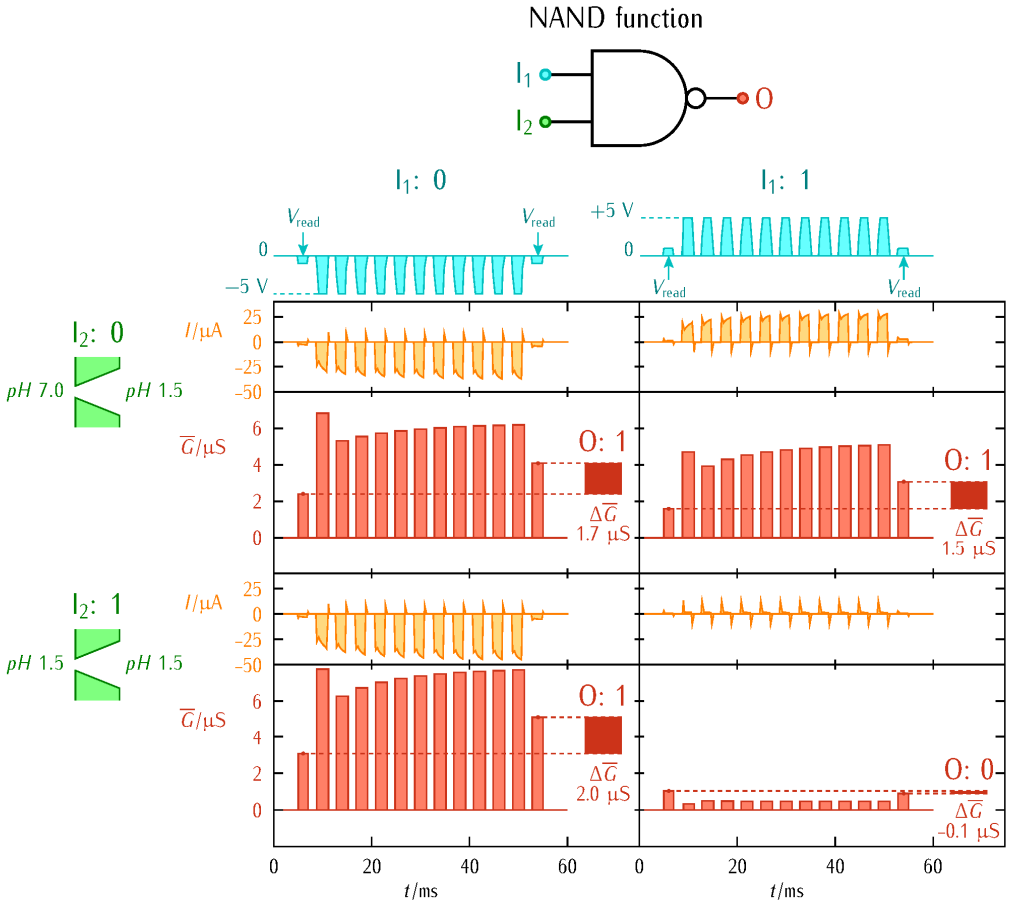

Fig. 3. The combination of the sign of the voltage V with pH_{tip} (*inputs* I_1 and I_2) gives a *NAND* logic response in terms of the membrane conductance (*output* O) for the case of 100 mM KCl solutions. The correspondence of *inputs* 0 and 1 with the *pH* (*left*) and voltage (*top*) values is shown. As in Fig. 2, the sequences of negative and positive voltage pulses give the average conductance difference $\Delta\overline{G}$ that characterizes the membrane response for the different configurations. In this case, three conductance potentiations are obtained.

Fig. 4 shows that a *XOR* logical function can also be obtained for the case of identical *pH* values ($pH_{tip} = pH_{base}$) and solution concentrations ($c_{tip} = c_{base}$) in symmetrical solutions (Fig. 1(b)). Here, the dependence of the surface pore charge on the *pH* provides a chemical rather than an electrical gating [30] that results in two conductance potentiations for inputs (0, 1) and (1, 0) only. The *XOR* function is usually difficult to implement because only one of the *input* variables must be 1 for the *output* variable to be 1.

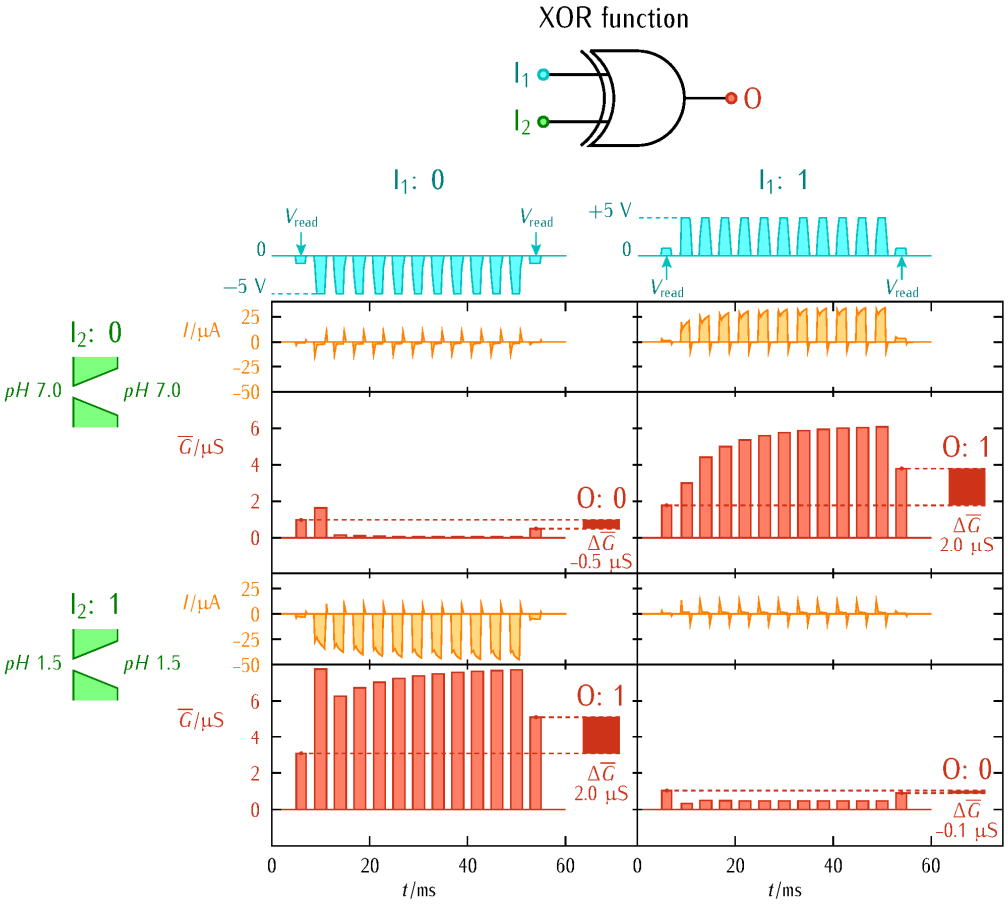

Fig. 4. The combination of the sign of the voltage with the *pH* in symmetrical solutions (*inputs*) give a *XOR* logic response in terms of the membrane conductance (*output*) for 100 mM KCl solutions. As in Fig. 2, the sequences of negative and positive voltage pulses give the average conductance difference $\Delta\bar{G}$ that characterizes the outputs. Two conductance potentiations are obtained here.

Fig. 5 shows a *Feynman* reversible logical function obtained by the combination of a *YES* function with the *XOR* function of Fig. 4 sharing one common *input* (voltage). The membrane logical response allows the univocal determination of the two *inputs* from the two *outputs*, as shown by the reversible truth table of Fig. 5. Note that only one *pH*, common to both external solutions, should be changed in the functional implementations of Figs. 4 and 5 that have also a common ionic concentration. This experimental fact permits a simple chemical switching that should facilitate the membrane reconfiguration under continuous operation.

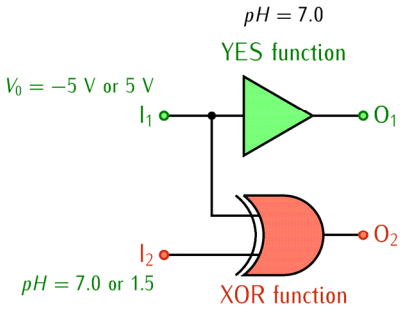

Input		Output: $\lvert\Delta\bar{G}\rvert$/μS	
$I_1 \equiv V_0$/V	$I_2 \equiv pH$	O_1	O_2
−5 (**0**)	7.0 (**0**)	0.5 (**0**)	0.5 (**0**)
+5 (**1**)	7.0 (**0**)	2.0 (**1**)	2.0 (**1**)
−5 (**0**)	1.5 (**1**)	0.5 (**0**)	2.0 (**1**)
+5 (**1**)	1.5 (**1**)	2.0 (**1**)	0.1 (**0**)

Fig. 5. Scheme of the *Feynman* reversible logical function implemented by the combination of the *YES* function in the scheme and the *XOR* function of Fig. 4. The truth table of this reversible logics uses the sign of the voltage amplitude V_0 and the solution *pH* as the two *inputs* variables.

The two *output* variables are the respective conductance potentiations characteristic of the *YES* and *XOR* functions.

The complete set of logical responses (*AND*, *NAND*, *XOR*, and *Feynman*) shown here involves electrical (voltage and current) and chemical (ionic concentration and *pH*) signals. Remarkably, a broad range of functionalities can be implemented on the basis of the *asymmetries* of the external solutions (*pH* and ionic concentration) and the membrane (geometry and axially distributed charge). These asymmetries provide the rectifying and memory properties of the nanofluidic diodes [1-3,29,31] that eventually give the different neuromorphic logical responses. Interestingly, symmetry-breaking combinations of *pH* and ionic concentrations are also characteristic of biomimetic and biological membranes [14,24,25,37-39], which should facilitate practical applications in biosystems.

As suggestions for future work, it is possible to use *three* rather than two different *pH* values leading to negative, zero, and positive pore surface charges [30]. This procedure would allow the implementation of *multivalued* logical functions on the basis of the multiple membrane conductances obtained, as previously demonstrated by the functionalization of polyprotic acid chains on the nanopore surface [40]. Also, the robust behavior of series and parallel membranes arrangements recently demonstrated [27] should make possible to process multiple *pH* and ionic concentration signals in other iontronics circuits.

4. Model simulations

As a convenient modeling tool, we present now simulations of the conductance potentiation/depression and logical responses. The model equations constitute a significant extension of our previous theoretical work [26] and allow the exploration of other systems in terms of directly accessible experimental parameters: the voltage pulse characteristics, ionic

concentrations, and *pH* values. Numerical models and simulations focused on the theory of transport phenomena have recently been presented by other authors [35,41].

Note that we do not attempt to describe quantitatively a particular set of data. Rather, we give some general equations that can be useful for a qualitative description of the system response to voltage pulses under different conditions. For the sake of concreteness, we consider first that the pore is negatively charged, so that the main electrical carriers are the cations, and assume that the voltage signal is applied to the pore tip. The conical pore asymmetry resulting in current rectification is accounted for by considering two relaxation times, τ_{+0} and τ_{-0}, for voltages $V > 0$ and $V < 0$, as experimentally observed [26]. These different times arise from the distinct ionic concentrations of the cone tip and base solutions, together with the fact that the cations enter the pore tip from the left solution at $V > 0$ and the cone base from the right solution at $V < 0$ (Fig. 1(a)). Note that, while the external solution concentrations may be equal, the cation concentrations at the conical pore extremes should be different due to the distinct fixed charge concentrations X_+ (*tip*) and X_- (*base*) [26]. Thus, because of the local electroneutrality condition, the cation concentrations should be of the same order of magnitude of X_+ and X_- at the pore tip and base, respectively. This condition permits to express the pore charge volume concentration as $X_j = 2|\sigma|/(Fa_j)$ (j = +,–), where σ is the surface charge density [26].

For the negatively charged pore, the cation concentration can be regarded as the state variable. Thus, the pore conductance relaxation should follow that of the cation concentration, which is described by the local continuity equation. By assuming that cations enter and leave the pore by the ionic conduction due to a constant electric field (V_0 / L), where V_0 is the voltage and L is the membrane thickness, this equation gives the following relaxation times for the tip and base ionic solutions [26]:

$$\tau_{+0} \approx \frac{X_+\left(L^2/D\right)}{c_0 F V_0/(RT)} \tag{1a}$$

$$\tau_{-0} \approx \frac{X_-\left(L^2/D\right)}{c_0 F V_0/(RT)} \tag{1b}$$

where F is the Faraday constant, R is the gas constant, T is the temperature, c_0 is the ionic concentration in the external solution, and D is the diffusion coefficient. Note that, because X_+/X_- is approximately given by the pore radii ratio $a_-(base)/a_+(tip) \approx 10-100$, the respective relaxation times of the ionic solutions at the cone tip and base can be different [26].

We consider now the voltage pulse

$$V(t) = \begin{cases} 0, & t < t_0 \\ V_{\text{on}}, & t_0 < t < t_0 + \Delta t \\ 0, & t > t_0 + \Delta t \end{cases} \tag{2}$$

where t_0 is a reference time for the onset of the voltage pulse V_{on}, which can be positive or negative, that is applied during a time interval Δt. A sequence of N pulses can be obtained by applying a voltage function $V(t)$ with a time period T. The membrane conductance $G_j(t)$ should follow the voltage changes with a characteristic relaxation time τ_j

$$\frac{\mathrm{d}G_j(t)}{\mathrm{d}t} = -\frac{\left[G_j(t) - G_j^{\mathrm{f}}\right]}{\tau_j}, \quad j = +, -, \text{off} \tag{3}$$

where G_j^{f} are the limiting quasi-steady state conductances [26]. Note that different pore relaxation processes at the pore tip (+) and base (–) should be expected for the distinct signs of the voltage pulse V_{on}. Experimentally, a third characteristic time τ_{off} characterizes the cation

concentration relaxation when the voltage $V(t)$ is switched off, so that the conductance relaxation time can be expressed as

$$\tau_j = \begin{cases} \tau_{\text{off}}, & t < t_0 \\ \tau_{j0}, & t_0 < t < t_0 + \Delta t \\ \tau_{\text{off}}, & t > t_0 + \Delta t \end{cases} \tag{4}$$

Thus, in order to obtain the membrane response to a sequence of voltage pulses, we should integrate Eq. (3) separately over each time window defined in Eq. (2), having in mind the different initial and quasi-steady state conductances involved in the distinct windows.

When a square voltage pulse of amplitude V_{on} is applied, the initial conductance G_{t_0} evolves towards the quasi-steady state value G_j^{f} corresponding to this voltage. After the voltage is switched off, however, the conductance attempts to recover the initial value G_{t_0} until a new pulse is applied, thus reestablishing the external driving process of Eq. (2). For the first voltage signal period (the reading period for the conductance before the potentiation/depression scheme) and by taking the reference time $t_0 = 0$, the time-dependent membrane conductance is

$$\frac{G_{\text{read}}(t)}{G_+^{\text{f}}} = \begin{cases} r_{\text{off}}, & t \le 0 \\ r_{\text{read}} + (r_{\text{off}} - r_{\text{read}})\exp(-t/\tau_{+0}), & 0 < t \le T/2 \\ r_{\text{off}} + \left[G(T/2)/G_+^{\text{f}} - r_{\text{off}} \right] \exp\left[-(t - T/2)/\tau_{\text{off}} \right], & T/2 < t \le T \end{cases} \tag{5}$$

where we have introduced the conductance ratios $r_{\text{read}} = G_{\text{read}}^{\text{f}} / G_+^{\text{f}}$ and $r_{\text{off}} = G_{t_0} / G_+^{\text{f}}$ in terms of the reference conductance G_+^{f}.

The above general scheme is applied to the subsequent signal periods considering that, for each new time integration, the *initial* conductance corresponds to the *final* conductance reached at the end of the previous integration. Thus, the conductances corresponding to the *n*-th period of the potentiation (+) and depression (–) schemes are:

$$\frac{G_+(t)}{G_+^{\mathrm{f}}}=\begin{cases}1+\left[\dfrac{G_+(nT)}{G_+^{\mathrm{f}}}-1\right]\exp(-(t-nT)/\tau_{+0}),\ nT<t\le nT+T/2\\ r_{\mathrm{off}}+\left[\dfrac{G_+(nT+T/2)}{G_+^{\mathrm{f}}}-r_{\mathrm{off}}\right]\exp\left[-(t-nT-T/2)/\tau_{\mathrm{off}}\right),\ nT+T/2<t\le(n+1)T\end{cases}$$

(6a)

$$\frac{G_-(t)}{G_+^{\mathrm{f}}}=\begin{cases}r_-+\left[\dfrac{G_-(nT)}{G_+^{\mathrm{f}}}-r_-\right]\exp(-t/\tau_{-0}),\ nT<t\le nT+T/2\\ r_{\mathrm{off}}+\left[\dfrac{G_-(nT+T/2)}{G_+^{\mathrm{f}}}-r_{\mathrm{off}}\right]\exp\left[-(t-T/2)/\tau_{\mathrm{off}}\right),\ nT+T/2<t\le(n+1)T\end{cases}\tag{6b}$$

In Eqs. (6a) and (6b), we have introduced the conductance ratio $r_- = G_-/G_+^{\mathrm{f}}$. Following the potentiation/depression sequences of Eqs. (6a) and (6b), a reading pulse analog to that of Eq. (5) is applied. In this case, however, the initial conductance is not G_{t_0} but that achieved at the end of the potentiation/depression sequence.

From the time-dependent membrane conductance $G_j(t)$, the current through the membrane can be obtained as $I_j(t)=G_j(t)V(t)$, where $V(t)$ can be a sequence of positive (j = +) or negative ($j=-$) voltage pulses. For the sake of comparison between different experimental conditions, it is convenient to define a reference steady state current as $I_+^{\mathrm{f}}=G_+^{\mathrm{f}}V_+$. In this way, a generic current $I_*=G_*V_*$ can be scaled to the reference current $I_+^{\mathrm{f}}=G_+^{\mathrm{f}}V_+$ as

$$\frac{I_+^{\mathrm{f}}}{I_*}=\frac{G_+^{\mathrm{f}}V_+}{G_*V_*}=\frac{\sqrt{X^2+4c_0^{\,2}}}{\sqrt{X^2+4c_*^{\,2}}}\frac{D_0V_+}{D_*V_*}\tag{7}$$

so that the relative effects of ionic concentration (c_0 and c_*) and voltage amplitude (V_+ and V_*) can be predicted. In Eq. (7), the Donnan ionic equilibrium has been assumed to relate the inside pore and external solution concentrations, where X is a typical fixed charge concentration

[26,31]. This physical model allows a qualitative description of both the *I–V* curves and the time-dependent currents observed with different pulse sequences.

The model of Eqs. (5) and (6) incorporates the conductance ratios r_{read}, r_{off}, and r_{-}, together with the relaxation times τ_{j0} (j = +, –; here, τ_{read} is assumed to be equal to τ_{j0}) and τ_{off}, as the input parameters of the potentiation conductance curves. Also, it permits to simulate the different logical functions obtained and explore other configurations and membrane responses on the basis of the above analytical equations. Here, we will define $V_{\text{on}} < 0$ and $V_{\text{on}} > 0$ as logical *inputs* 0 and 1, respectively. For the logical *output*, we will take the absolute value $\left|\Delta\overline{G}\right|$ of the difference between the average conductance measured with two reading pulses, one just before the potentiation/depression sequence, and the other just after the sequence.

To show the effects of ionic concentration and *pH*, Figs. 6 and 7 give the model results obtained for the *AND* and *XOR* logic functions, respectively; the experimental *NAND* logic function can also be reproduced by the theoretical simulations (not shown here). Note that the capacitive peaks in the conductance, which are observed at the onset of the pulses (Figs. 2–4), are ignored. At the beginning and end of each voltage sequence, *read* pulses of amplitude $V_{\text{read}} = \pm 1$ V are applied, with the pulse sequences $V_{\text{on}} = \pm 5$ V. Note however that other current *vs*. time curves, conductance potentiation/depression, and logical responses could be obtained by exploring different experimental configurations.

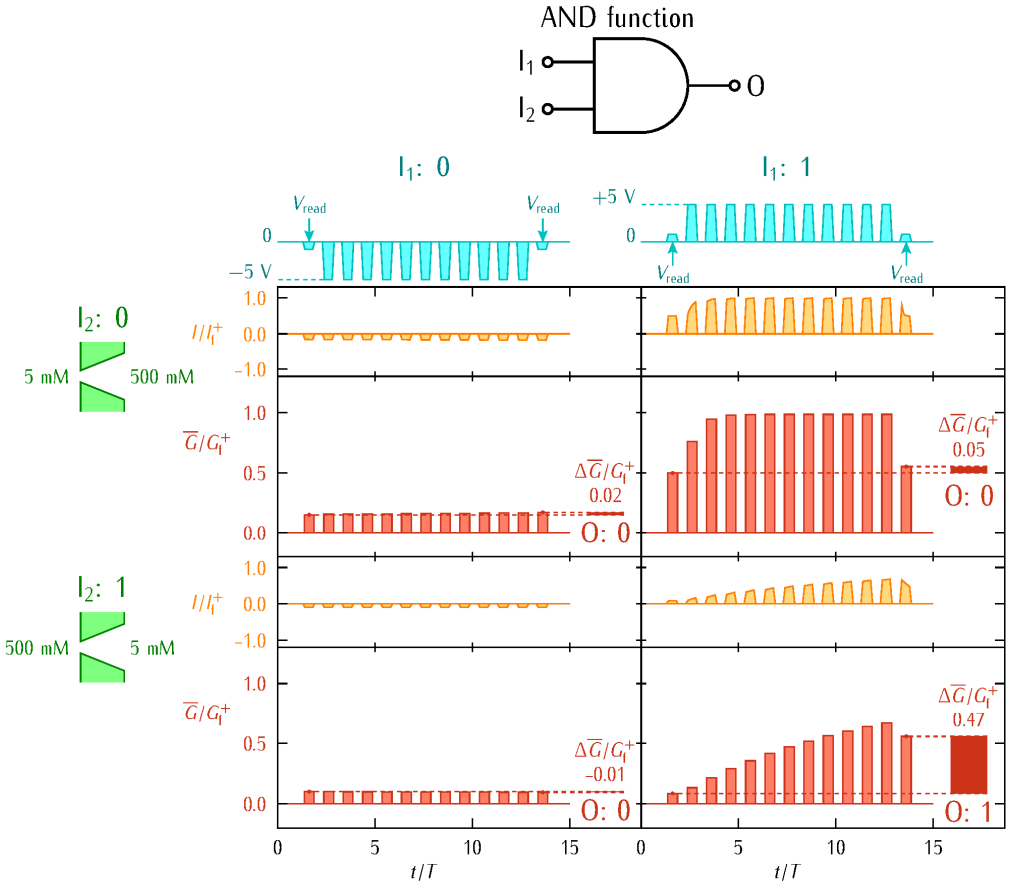

Fig. 6. The current *vs*. time curves, conductance potentiation, and logical responses obtained for the *AND* logical function with the model. The *inputs* are the signs of the voltage and the concentration difference. The *output* is the absolute value of the average conductance change between the initial and read voltage pulses. Note that the time, the current, and the conductance difference are scaled to the reference values T, I_+^f and G_+^f, respectively. The simulation parameters are as follows: (*i*) Configuration 5/500 mM KCl for the positive voltage sequence, $T/\tau_{+0}=3.4$, $r_{\text{off}}=0.5$, and $r_{\text{read}}=0.5$, and $T/\tau_{\text{off}}=0.1$, with a reference ionic concentration $c_0=5$ mM KCl; for the negative voltage sequence, $T/\tau_{-0}=0.01$, $r_{\text{off}}=0.15$, $r_{\text{read}}=0.5$, and $r_{-}=0.4$, and $T/\tau_{\text{off}}=0.01$, with a reference ionic concentration $c_0=500$ mM KCl. (*ii*) Configuration 500/5 mM KCl for the positive voltage sequence, $T/\tau_{+0}=0.2$, $r_{\text{off}}=0.08$, and $r_{\text{read}}=0.1$, and $T/\tau_{\text{off}}=0.01$,with a reference ionic concentration $c_0=500$ mM KCl; for the

negative voltage sequence, $T/\tau_{-0} = 0.05$, $r_{off} = 0.1$, $r_{read} = 0.1$, and $r_{-} = 0.07$, and $T/\tau_{off} = 0.1$,with a reference ionic concentration $c_0 = 5$ mM KCl.

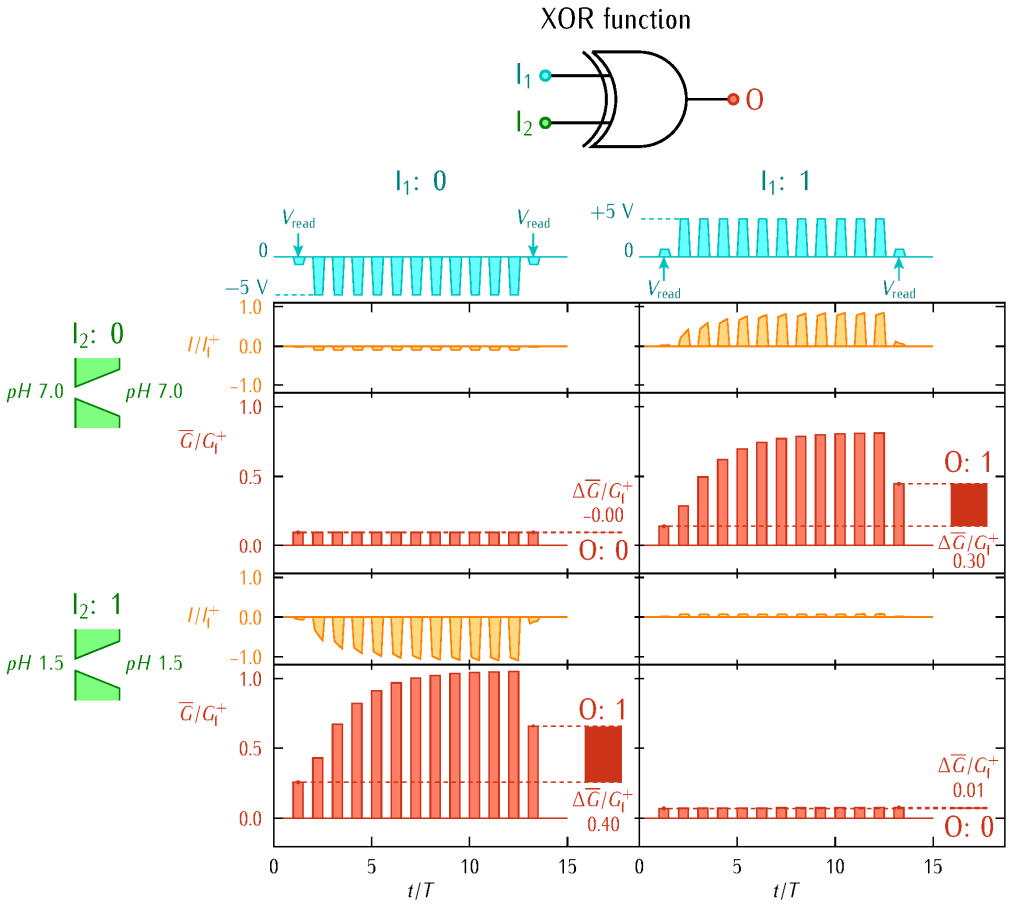

Fig. 7. The current *vs*. time curves, conductance potentiation, and logical responses obtained for the *XOR* logical function with the model. The *inputs* are the sign of the voltage and the *pH* in the external solutions. The *output* is the absolute value of the average conductance change between the initial and read voltage pulses. Note that the time, the current, and the conductance difference are scaled to the reference values T, I_{+}^{f} and G_{+}^{f}, respectively. The simulation parameters are as follows: (*i*) For *pH* = 7.0 and the positive voltage sequence, $T/\tau_{+0} = 0.8$, $T/\tau_{off} = 0.2$, and $r_{off} = 0.07$; for the negative voltage sequence, $T/\tau_{-0} = 0.002$, $T/\tau_{off} = 0.2$, $r_{off} = 0.1$, and $r_{-} = 0.01$. In both cases, $r_{read} = 0.2$. (*ii*) For *pH* = 1.5 and the positive voltage

sequence, $T/\tau_{+0} = 0.002$, $T/\tau_{\text{off}} = 0.2$, and $r_{\text{off}} = 0.007$; for the negative voltage sequence, $T/\tau_{-0} = 0.8$, $T/\tau_{\text{off}} = 0.2$, $r_{\text{off}} = 0.07$, and $r_{-} = 1.3$. In both cases, $r_{\text{read}} = 0.4$.

5. Conclusions

Surface charge-regulated ion transport in soft nanostructures can mimic some of the functionalities of cell membranes and is of current interest to iontronics hybrid devices [5,7,12-16,18,19,23,30,34]. Here, we have shown that the memristive conductance potentiation of nanofluidic diodes allows to evoke a broad set of logical functions with timing and responses different than those of the electrical steady-state logics. The membrane response can be modulated not only by the amplitude and frequency of the driving oscillatory signal [9] but also by the ionic concentration and *pH* values of the external solutions (Fig. 1), reminiscent of physiological processes in cell membranes [24,25]. These qualitative links between liquid-state ionic memristors and biological ion channels should facilitate signal conversion and information processing in bioengineering and health sciences. Suggestions for future work and model simulations are also included to explore future applications.

As a proof of concept, different Boolean (*AND*, *NAND*, and *XOR*) and reversible (*Feynman*) logical functions are obtained by simple external reconfigurations of the nanofluidic diode states (Figs. 2–5). The *NAND* function is *universal*, thus allowing the implementation of other functions by appropriate combinations. Also, the *XOR* function is usually difficult to realize in practical applications. The *Feynman* function suggests that other reversible logic responses could be evoked by different combinations of experimental *inputs* and *outputs*. The fact that all these functionalities use the same physical environment, a conventional electrochemical cell with the usual chemical (*pH* and ionic concentrations) and electrical

(voltage and current) signals, suggests new opportunities for sensing and information processing in liquid state iontronics.

Credit author statement

Sergio Portillo: Conceptualization (equal); Formal analysis (equal); Investigation (equal); Methodology (equal); Visualization (equal); Writing – review & editing (equal). **Javier Cervera:** Conceptualization (equal); Formal analysis (equal); Funding acquisition (equal); Project administration (lead); Supervision (equal); Visualization (equal); Writing – review & editing (equal). **Salvador Mafe:** Conceptualization (lead); Formal analysis (equal); Funding acquisition (equal); Supervision (equal); Writing – original draft (lead). **Patricio Ramirez:** Conceptualization (lead); Data curation (lead); Formal analysis (equal); Investigation (equal); Methodology (lead); Resources (equal); Visualization (equal); Writing – review & editing (equal).

Declaration of competing interest

The authors declare that they have no known competing financial interests or personal relationships that could have appeared to influence the work reported in this paper.

Data availability

Data will be made available on reasonable request.

Acknowledgment

S.P., J.C., S.M., and P.R. acknowledge the support from the *Ministerio de Ciencia e Innovación* (Spain) and the European Regional Development Funds (FEDER), project PID2022-

139953NB-I00. We thank Dr. Saima Nasir and Dr. Mubarak Ali for preparing the membrane samples and Prof. Wolfgang Ensinger for his assistance.

References

[1] P. B. Peters, R. van Roij, M. Z. Bazant, P. M. Biesheuvel, Analysis of electrolyte transport through charged nanopores, Phys. Rev. E 93 (2016) 053108. https://doi.org/10.1103/PhysRevE.93.053108.

[2] Y. Green, Y. Edri, G. Yossifon, Asymmetry-induced electric current rectification in permselective systems, Phys. Rev. E 92 (2015) 033018. https://doi.org/10.1103/PhysRevE.92.033018.

[3] T.-W. Lin, J.-P. Hsu, C.-Y. Lin, S. Tseng, Dual pH gradient and voltage modulation of ion transport and current rectification in biomimetic nanopores functionalized with a pH-tunable polyelectrolyte, J. Phys. Chem. C 123 (2019) 12437−12443. https://doi.org/10.1021/acs.jpcc.8b11707.

[4] C.-Y. Lin, E. T. Acar, J. W. Polster, K. Lin, J.-P. Hsu, Z. S. Siwy, Modulation of charge density and charge polarity of nanopore wall by salt gradient and voltage, ACS Nano 13 (2019) 9868−9879. https://doi.org/10.1021/acsnano.9b01357.

[5] T. M. Kamsma, W. Boon, Q. T. ter Rele, C. Spitoni, R. van Roij, Iontronic neuromorphic signaling with conical microfluidic memristors, Phys. Rev. Lett. 130 (2023) 268421. https://doi.org/10.1103/PhysRevLett.130.268401.

[6] P. Robin, N. Kavokine, L. Bocquet, Modeling of emergent memory and voltage spiking in ionic transport through angstrom-scale slits, Science 373 (2021) 687. https://doi.org/10.1126/science.abf79.

[7] P. Robin, T. Emmerich, A. Ismail, A. Niguès, Y. You, G.-H. Nam, A. Keerthi, A. Siria, A. K. Geim, B. Radha, L. Bocquet, Long-term memory and synapse-like dynamics in two-dimensional nanofluidic channels, Science 379 (2023) 161−167. https://doi.org/10.1126/science.adc9931.

[8] A. Noy, Z. Li, S. B. Darling, Fluid learning: Mimicking brain computing with neuromorphic nanofluidic devices, Nano Today 53 (2023) 102043. https://doi.org/10.1016/j.nantod.2023.102043.

[9] P. Ramirez, V. Gomez, J. Cervera, S. Mafe, J. Bisquert, Synaptical tunability of multipore nanofluidic memristors, J. Phys. Chem. Lett. 14 (2023) 10930−10934. https://doi.org/10.1021/acs.jpclett.3c02796.

[10] K. Xiao, L. Wen, L. Jiang, Biomimetic solid-state nanochannels: From fundamental research to practical applications, Small 12 (2016) 2810−2831. https://doi.org/10.1002/smll.201600359.

[11] A. Paul, N. R. Aluru, Nanoscale electrohydrodynamic ion transport: Influences of channel geometry and polarization-induced surface charges, Phys. Rev. E 109 (2024) 025105. https://doi.org/10.1103/PhysRevE.109.025105.

[12] D. Duleba, R. P. Johnson, Iontronics: From fundamentals to ion controlled devices, Curr. Opin. Electrochem. 34 (2022) 100989. https://doi.org/10.1039/D3FD90046K.

[13] Z. S. Siwy, M. L. Bruening, S. Howorka, Nanopores: synergy from DNA sequencing to industrial filtration – small holes with big impact, Chem. Soc. Rev. 52 (2023) 1983–1994. https://doi.org/10.1039/D2CS00894G.

[14] Y. Hou, Y. Ling, Y. Wang, M. Wang, Y. Chen, X. Li, X. Hou, Learning from the brain: Bioinspired nanofluidics, J. Phys. Chem. Lett. 14 (2023) 2891−2900. https://doi.org/10.1021/acs.jpclett.2c03930.

[15] Y. Hou, X. Hou, Bioinspired nanofluidic iontronics, Science 373 (2021) 628−629. https://doi.org/10.1126/science.abj0437.

[16] G. Perez-Mitta, A. G Albesa, C. Trautmann, M. E. Toimil-Molares, O. Azzaroni, Bioinspired integrated nanosystems based on solid-state nanopores: "iontronic" transduction of biological, chemical and physical stimuli, Chem. Sci. 8 (2017) 890−913. https://doi.org/10.1039/C6SC04255D.

[17] G. Pérez-Mitta, M. E. Toimil-Molares, C. Trautmann, W. A. Marmisollé, O. Azzaroni,

Molecular Design of Solid-State Nanopores: Fundamental Concepts and Applications, 31 (2019) 1901483. https://doi.org/10.1002/adma.201901483.

[18] M. Tagliazucchi, I. Szleifer, Transport mechanisms in nanopores and nanochannels: can we mimic nature?, Mat. Today 18 (2015) 131–142. https://doi.org/10.1016/j.mattod.2014.10.020.

[19] T. Ma, J.-M. Janot, S. Balme, Track-etched nanopore/membrane: From fundamental to applications, Small Methods 4 (2020) 2000366. https://doi.org/10.1002/smtd.202000366.

[20] J. Bisquert, Current-controlled memristors: Resistive switching systems with negative capacitance and inverted hysteresis, Phys. Rev. Applied 20 (2023) 044022. https://doi.org/10.1103/PhysRevApplied.20.044022.

[21] J. Bisquert, Inductive and capacitive hysteresis of current-voltage curves: Unified structural dynamics in solar energy devices, memristors, ionic transistors and bioelectronics, Phys. Rev. X Energy 3 (2024) 011001. https://doi.org/10.1103/PRXEnergy.3.011001.

[22] T. Xiong, C. Li, X. He, B. Xie, J. Zong, Y. Jiang, W. Ma, F. Wu, J. Fei, P. Yu, L. Mao, Neuromorphic functions with a polyelectrolyte-confined fluidic memristor, Science 379 (2023) 156–161. https://doi.org/10.1126/science.adc9150.

[23] T. M. Kamsma, J. Kim, K. Kim, R. van Roij, Brain-inspired computing with fluidic iontronic nanochannels, Proc. Nat. Acad. Sci. 121 (2024) e2320242121. https://doi.org/10.1073/pnas.2320242121.

[24] B. Hille, Ion Channel of Excitable Membranes. Sinauer Associates: Sunderland, Massachusetts, 2001.

[25] J. Cervera, M. Levin, S. Mafe, Bioelectricity of non-excitable cells and multicellular pattern memories: Biophysical modeling, Phys. Rep. 1004 (2023) 1–31. https://doi.org/10.1016/j.physrep.2022.12.003.

[26] J. Cervera, S. Portillo, P. Ramirez, S. Mafe, Modeling of memory effects in nanofluidic diodes, Phys. Fluids 36 (2024) 047129. https://doi.org/10.1063/5.0204219.

[27] P. Ramirez, S. Portillo, J. Cervera, J. Bisquert, S. Mafe, Memristive arrangements of nanofluidic pores, Phys. Rev. E 109 (2024) 044803. https://doi.org/10.1103/PhysRevE.109.044803.

[28] P. Apel, Track etching technique in membrane technology, Radiat. Meas. 34 (2001) 559–566. https://doi.org/10.1016/S1350-4487(01)00228-1.

[29] Z. Siwy, A. Fulinski, Fabrication of a synthetic nanopore ion pump, Phys. Rev. Lett. 89 (2002) 198103. https://doi.org/10.1103/PhysRevLett.89.198103.

[30] P. Ramirez, V. Garcia-Morales, V. Gomez, M. Ali, S. Nasir, W. Ensinger, S. Mafe, Hybrid circuits with nanofluidic diodes and load capacitors, Phys. Rev. Applied 7 (2017) 064235. https://doi.org/10.1103/PhysRevApplied.7.064035.

[31] J. Cervera, B. Schiedt, R. Neumann, S. Mafe, P. Ramirez, Ionic conduction, rectification, and selectivity in single conical nanopores, J. Chem. Phys. 124 (2006) 104706. https://doi.org/10.1063/1.2179797.

[32] D. Wang, M. Kvetny, J. Liu, W. Brown, Y. Li, G.Wang, Transmembrane potential across single conical nanopores and resulting memristive and memcapacitive ion transport, J. Am. Chem. Soc. 134 (2012) 3651−3654.

https://doi.org/10.1021/ja211142e.

[33] P. Ramirez, J. Cervera, S. Nasir, M. Ali, W. Ensinger, S. Mafe, Memristive switching of nanofluidic diodes by ionic concentration gradients, Colloid Surface A 698 (2024) 134525. https://doi.org/10.1016/j.colsurfa.2024.134525.

[34] Y. Ling, L. Yu, Z. Guo, F. Bian, Y. Wang, X. Wang, Y. Hou, X. Hou, Single-pore nanofluidic logic memristor with reconfigurable synaptic functions and designable combinations, J. Am. Chem. Soc. 146 (2024) 14558−14565. https://doi.org/10.1021/jacs.4c01218.

[35] Z. Liu, L. Ma, H. Zhang, J. Zhuang, J. Man, Z. S. Siwy, Y. Qiu, Dynamic Response of Ionic Current in Conical Nanopores, ACS Appl. Mater. Interfaces 16 (2024) 30496−30505. https://doi.org/10.1021/acsami.4c02078.

[36] S. Portillo, J. A. Manzanares, Ramirez, J. Bisquert, S. Mafe, J. Cervera, pH-dependent Effects in Nanofluidic Memristors, J. Phys. Chem. Lett. 15 (2024) 7793−7798. https://doi.org/10.1021/acs.jpclett.4c01610.

[37] A. Alcaraz, E. M. Nestorovich, M. Aguilella-Arzo, V. M. Aguilella, S. M. Bezrukov, Salting out the ionic selectivity of a wide channel: the asymmetry of OmpF, Biophys. J. 87 (2004) 943–957. 943–957. https://doi.org/10.1529/biophysj.104/043414.

[38] M. Queralt-Martin, E. Garcia-Gimenez, V. M. Aguilella, P. Ramirez, S. Mafe, A. Alcaraz, Electrical pumping of potassium ions against an external concentration gradient in a biological ion channel, Appl. Phys. Lett. 103 (2013) 043707. https://doi.org/10.1063/1.4816748.

[39] V. M. Aguilella, M. Queralt-Martín, M. Aguilella-Arzo, A. Alcaraz, Insights on the permeability of wide protein channels: measurement and interpretation of ion selectivity, Integr. Biol. 3 (2011) 159–172. https://doi.org/10.1039/C0IB00048E.

[40] M. Ali, S. Mafe, P. Ramirez, R. Neumann, W. Ensinger, Logic gates using nanofluidic diodes based on conical nanopores functionalized with polyprotic acid chains, Langmuir 25 (2009) 11993–11997. https://doi.org/10.1021/la902792f.

[41] W. Wang, Y. Liang, Y. Ma, D. Shi, Y. Xie, Memristive Characteristics in an Asymmetrically Charged Nanochannel, J. Phys. Chem. Lett. 15 (2024) 6852−6858. https://doi.org/10.1021/acs.jpclett.4c00488.